European Conference on Computational Fluid Dynamics
ECCOMAS CFD 2006
P. Wesseling, E. Oñate and J. Périaux (Eds)

SIMULATIONS OF MERGING IN A TWO CO-ROTATING VORTEX SYSTEM

L. Nybelen*, H. Moet and R. Paoli

*Centre Européen de Recherche et de Formation Avancée en Calcul Scientifique,
42, Avenue Gaspard Coriolis, 31057 Toulouse Cedex 01, France
e-mail: nybelen@cerfacs.fr
web page: http://www.cerfacs.fr

Key words: Direct Numerical Simulation DNS, Large-Eddy Simulation LES, vortex merging, elliptic instability

Abstract. *All aircraft shed, as a consequence of lift, a wake ("vorticity sheet") which rapidly rolls up into several concentrated vortices at a distance of a few chords behind the trailing edge of the wing. A simplified configuration has been adopted to understand the physical mechanisms characterizing the merging process in the extended near-field. This consists in two co-rotating and symmetric (i.e same core size a and circulation* Γ*) vortices, corresponding to the two vortices generated at wing and flap tip, respectively. Both the Lamb-Oseen and the Jacquin[22] VM2 vortex models were used as numerical initial conditions. Two dimensional Direct Numerical Simulations (DNS) were first conducted at low Reynolds numbers to study the merging in stable conditions. A so-called convective stage is identified which is critical in the stable merging process. It starts when the ratio between the vortex core size a and the separation distance b of the two vortices reaches the critical value* $a/b \sim 0.24$ *for the Reynolds numbers considered (*$750 < Re_\Gamma < 10000$*).*
It is known that the vortex system might experience an elliptic short wavelength instability during the merging process at high Reynolds numbers[14] . A second set of three-dimensional simulations (DNS/LES) was then carried out to analyse the development of such a short wavelength instability. The development of the instability was analysed by either looking at the flow topology or by tracking the energy spectrum of the system. The resulting (unstable) vortex has a two-scale tangential velocity profile as in the case of two-dimensional (stable) merging. However the unstable merging is faster than the stable merging.

1 INTRODUCTION

The wake of an aircraft is composed of several intense vortices which might persist for a few minutes in the atmosphere. They may be hazardous for other aircraft encountering the wake, in particular during the take-off and landing phases. One needs to characterize the structure of hazardous trailing vortices to develop new concepts to accelerate

the decay. It consists in understanding the generic physical phenomena acting, from the generation of the wake down to the far-field, where a vortex encounter with a following aircraft would take place. The present study focuses on the dynamics in the extended near-field, from just downstream of the aircraft wing generating a vortex sheet, to the region where the vortex system remaining in the far-field is generally formed by a single large vortex behind each wing. The main physical phenomenom occuring in the extended near field is the merging of the co-rotating vortices, generated at flap and wing tip.
The merging of two co-rotating vortices has received much attention over the last few years. Cerretelli and Williamson[20] shown in their experiments, that this physical phenomenon can be decomposed into four stages for low Reynolds number. They found that the merging is caused by a generation of an antisymmetric vorticity field during the process, inducing a velocity pushing one vortex to the other. Moreover, they have shown that the merging time is function to the Reynolds number and the initial characteristic ratio a/b, between the vortex core size and the separation distance. The influence of the Reynolds number on the 2D laminar merging was stutied by Ferreira and Pereira[23] , using Direct Numerical Simulations. They found that the mechanism can be decomposed into two stages for Reynolds number less than 500 and into four stages at higher Reynolds number, as in experiments of Cerretelli and Williamson[20] . It is well known in 2D case that the merging is onset when the characteristic ratio exceeded a critical value. Meunier[19] *et al.* established a quantitative criterion for the merging of a pair of equal co-rotating vortices. Leweke[14] *et al.* confirmed this result by experimental and numerical study. Moreover, they observed at high Reynolds number in their experiments a 3D elliptic instability, which generates small-scale turbulent motion leading to the merging. A theoretical prediction of this instability was established by Le Dizes and Laporte[16] . They obtained a formula of the growth rate during the linear regime as function of the initial ratio a/b and the Reynolds number. This theoretical approach was supported by DNS and LES.
The present numerical study focuses on the evolution of a co-rotating vortex pair using two vortex models : Lamb-Oseen vortex model and the Jacquin[22] VM2 vortex model. The first one is used to validate the new results by comparison with the previous studies (Leweke[14] *et al.*, Le Dizes and Laporte[16]). The second best fits a typical wake vortex in the extended near-field and was used for the first time in simulation of 2D laminar merging and also of the development of the 3D elliptic instability leading to an unstable merging.

2 GOVERNING EQUATIONS AND NUMERICAL MODEL

2.1 Governing equations

The nondimensional formulation of the 3D compressible Navier-Stokes equations reads

$$\begin{aligned} \frac{\partial \rho}{\partial t} + \frac{\partial (\rho u_j)}{\partial x_j} &= 0 \\ \frac{\partial (\rho u_i)}{\partial t} + \frac{\partial (\rho u_i u_j)}{\partial x_j} + \frac{\partial p}{\partial x_i} &= \frac{1}{Re} \frac{\partial \tau_{ij}}{\partial x_j} \\ \frac{\partial (\rho E)}{\partial t} + \frac{\partial [(\rho E + p) u_j]}{\partial x_j} &= \frac{1}{Re} \frac{\partial (u_i \tau_{ij})}{\partial x_j} - \frac{1}{Re\, Pr} C_p \frac{\partial q_j}{\partial x_j} \end{aligned} \tag{1}$$

where the nondimensional variables are: the density ρ, the velocity vector $(u_1, u_2, u_3)^T$, the pressure p, the total energy E, the heat flux vector $(q_1, q_2, q_3)^T$ given by Fourier's law, and the shear stress tensor τ_{ij}. The C_p coefficient is the specific heat at constant pressure. The nondimensional variables are defined as the local dimensional variables divided by a reference variable or a combination of the reference variables. The reference variables are: the density ρ_{ref}, the velocity a_{ref}, the pressure p_{ref}, the length l_{ref}, the temperature T_{ref}, the dynamic viscosity μ_{ref} and the specific heat $C_{p,ref}$. The reference Reynolds number is $Re = \rho_{ref} a_{ref} l_{ref} / \mu_{ref}$ while Pr stands for the Prandtl number (in the present simulation $Pr = 0.75$).

2.2 LES approach and subgrid scale model description

In the Large-Eddy Simulation (LES) approach the previous equations are filtered spatially, so that any variable $\phi(x)$ may be decomposed into a resolved (or large scale) part $\overline{\phi(x)}$ and a nonresolved (or subgrid scale) part $\phi''(x)$, with $\phi(x) = \overline{\phi(x)} + \phi''(x)$. This procedure may be obtained by a convolution integral of the variable with any filter function depending on a filter width Δ. Practically, the filter width is simply given by the computational mesh cell size Δ_x. For compressible flows, the Favre-filtered variables defined as $\phi(x) = \tilde{\phi}(x) + \phi'(x)$ are used, with $\tilde{\phi} = \overline{\rho\phi}/\overline{\rho}$. The dimensionless Favre-filtered equations are:

$$\begin{aligned} \frac{\partial \overline{\rho}}{\partial t} + \frac{\partial (\overline{\rho} \tilde{u}_j)}{\partial x_j} &= 0 \\ \frac{\partial (\overline{\rho} \tilde{u}_i)}{\partial t} + \frac{\partial (\overline{\rho} \tilde{u}_i \tilde{u}_j)}{\partial x_j} + \frac{\partial \overline{p}}{\partial x_i} &= \frac{1}{Re} \frac{\partial \tilde{\tau}_{ij}}{\partial x_j} + \frac{\partial \sigma_{ij}}{\partial x_j} \\ \frac{\partial (\overline{\rho} \tilde{E})}{\partial t} + \frac{\partial [(\overline{\rho} \tilde{E} + \overline{p}) \tilde{u}_j]}{\partial x_j} &= \frac{1}{Re} \frac{\partial \tilde{\tau}_{ij} \tilde{u}_i}{\partial x_j} + \frac{\partial \sigma_{ij} \tilde{u}_i}{\partial x_j} - \frac{1}{Re\, Pr} C_p \frac{\partial \tilde{q}_j}{\partial x_j} - \frac{\partial Q_j}{\partial x_j} \end{aligned} \tag{2}$$

where the subgrid scale (SGS) stress tensor $\sigma_{ij} = -(\overline{\rho u_i u_j} - \overline{\rho} \tilde{u}_i \tilde{u}_j)$ and the SGS heat flux $Q_j = \overline{\rho C_p T u_j} - \overline{\rho} C_p \tilde{T} \tilde{u}_j$ are to be modeled and where the following classical approximations (see Erlebacher[5] *et al.*) have been made:

- The Favre-filtered shear stress tensor is identified with the filtered shear stress tensor
- The Favre-filtered heat flux is identified with the filtered heat flux

- The filtered kinetic energy term $\overline{\rho K u_j}$ in the energy equation is approximated by $\overline{\rho}\tilde{K}\tilde{u}_j - \sigma_{ij}\tilde{u}_j$, where $K = 1/2 u_i u_i$ is the kinetic energy. The SGS momentum σ_{ij} and the SGS heat flux Q_j are modeled through the subgrid-scale eddy-viscosity concept:

$$\sigma_{ij} - \frac{1}{3}\sigma_{kk}\delta_{ij} = -2\mu_{sgs}\Big(\tilde{S}_{ij} - \frac{1}{3}\delta_{ij}\tilde{S}_{kk}\Big) \qquad (3)$$
$$Q_j = -\frac{\mu_{sgs}\, C_p}{Pr_t}\frac{\partial \Theta}{\partial x_j}$$

where μ_{sgs} is the SGS dynamic viscosity and $\tilde{S}_{ij}$ is the large scale strain rate tensor; while Pr_t is the turbulent Prandtl number, defining the modified temperature $\Theta = \tilde{T} - 1/(2\overline{\rho}C_v)\sigma_{kk}$, where C_v is the specific heat at constant volume.
The SGS viscosity model is based on the Structure Function model (Métais and Lesieur[6]) initially developed in spectral space (effective viscosity model) and then transposed into the physical space. The expression of the Structure Function is

$$\overline{F}_2(\vec{x}, \Delta, t) = \langle \|\vec{\tilde{u}}(\vec{x} + \vec{r}, t) - \vec{\tilde{u}}(\vec{x}, t)\| \rangle_{\|\vec{r}\|=\Delta} \qquad (4)$$

where Δ is the cutoff length and where $\langle\rangle$ denotes spatial averaging, here over the sphere of radius Δ. As the information brought by the model is local in space it leads to a poor estimation of the kinetic energy at the cutoff which may be improved by a suitable filtering in order to remove the influence of the large scales on the SGS viscosity. The procedure defined by Ducros[8] *et al.* is to apply (possibly n times) a discrete Laplacian high-pass filter to the velocity field before calculating the Structure Function. The optimum value of n found by Ducros[8] *et al.* for their simulations is $n = 3$. This value has also been used here. Finally, the Filtered Structure Function model reads:

$$\nu_{sgs} = \mu_{sgs}/\overline{\rho} = \nu_{sgs}(\vec{x}, \Delta, t) = \alpha^{(n)}\Delta\sqrt{\overline{F_2}^{(n)}(\vec{x}, \Delta, t)} \qquad (5)$$

where the superscript (n) indicates that the filter has been applied n times. The value of α used here is $\alpha^{(3)} = 0.00084$. The Structure Function model formulation of Métais and Lesieur[6] in spectral space insures that the SGS viscosity vanishes when there is no energy at the cutoff wavelength. This property is particularly important for the simulation of transitional flows as those of interest in the present paper.

3 NUMERICAL RESULTS

3.1 Framework and initial condition

The two-dimensional domain is defined by $L_x = L_y = 20b_0$ (b_0 is the reference length corresponding to the separation distance between the two co-rotating vortices wich form the initial vortex system, see Fig. 1), and consists of $N_x \times N_y = 401 \times 401$ grid points in the xy-plane (see Tab. 1). The mesh is regular in the region of interest for the dynamics of the vortex system, *i.e.* $D_p = L_{xp} \times L_{yp} = 1.2b_0 \times 1.2b_0$, with a grid resolution

$\Delta_x = \Delta_y = 7 \times 10^{-3} b_0$. The mesh is then streched far away to minimize the effects of the borders (see Fig. 1). Symmetry conditions were applied in both x and y direction.[7]
For the 3D temporal simulations, the computational domain in the transverse plane is the same as in the 2D case. The axial direction is periodic and the length as $L_z = 3\lambda_z = 1.4805 b_0$ where λ_z is the wavelength which corresponds to the elliptic instability, according to the theoretical prediction of Le Dizes and Laporte.[16] There are $N_z = 36$ points in the z-direction (or 12 points per wavelength, as suggested by Le Dizes and Laporte[16]); so that the total number of gridpoints in this case is $N_{tot} = 5788836$.).
Two co-rotating vortices with the same circulation and core size are placed in the computational domain (see Fig. 1), according to either the Lamb-Oseen or the Jacquin[22] VM2 vortex models.
The Lamb-Oseen vortex model (Gaussian) describes the structure of the vortex core with one length scale, defined by the radius r_c where the tangential velocity v_θ is maximum (Fig. 2). In a cylindrical coordinate system $(\vec{e_r}, \vec{e_\theta}, \vec{e_z})$, the velocity field of a single axisymmetric vortex is :

$$\begin{aligned} v_r(r,t) &= v_z(r,t) = 0 \\ v_\theta(r,t) &= \frac{\Gamma}{2\pi r}(1 - e^{-(\beta r/r_c)^2}) \end{aligned} \tag{6}$$

where $\beta = 1.256$. The circulation strength Γ is related to the maximum tangential velocity $V_0 \equiv v_\theta(r_c)$ following the relation $\Gamma = 2\pi\epsilon r_c V_0$ with $\epsilon = 1.398$.
The VM2 model[22] describes the structure of vortex core by means of two length scales, an internal core scale a_1 which corresponds to the r_c of Lamb-Oseen model (location of the maximum velocity) and an external core scale a_2, corresponding to the location where the vorticity vanishes (see Fig. 2). The flow in the internal core is characterized by solid body rotation $v_\theta(r) \sim r$ and behaves as a potential $(v_\theta(r) \sim 1/r)$ flow outside the external core $(r > a_2)$. In the intermediate zone $(a_1 < r < a_2)$, the velocity law follows a power law $v_\theta(r) \sim r^{-\alpha}$. In cylindrical coordinates $(\vec{e_r}, \vec{e_\theta}, \vec{e_z})$, the velocity field is :

$$\begin{aligned} v_r(r,t) &= v_z(r,t) = 0 \\ v_\theta(r,t) &= \frac{\Omega_0 r}{[1 + (r/a_1)^4]^{(1+\alpha)/4}[1 + (r/a_2)^4]^{(1-\alpha)/4}} \end{aligned} \tag{7}$$

where Ω_0 is the rotation rate of the internal core. The overall circulation of this vortex is given by :

$$\Gamma = 2\pi\Omega_0 {a_1}^2 \left(\frac{a_2}{a_1}\right)^{(1-\alpha)} \tag{8}$$

The VM2 vortex also has two velocity scales, an internal velocity $V_1 = \Omega_0 a_1$ and an external velocity $V_2 = \Gamma/2\pi a_2$. Through this study, the characteristics parameters $\alpha = 0.5$ and $a_2/a_1 = 10$, have been used as they are representative of aircraft wakes.[13]

As common practice in the analyses of two co-rotating vortices,[18],[14],[12],[19] the dispersion radius a is used to identify the vortex core size. This is defined as the second polar moment of vorticity with respect to the vorticity center (x_c, y_c) :

$$a^2 = \frac{1}{\Gamma} \langle [(x - x_c)^2 + (y - y_c)^2] \, \omega \rangle \tag{9}$$

The notation $\langle\rangle$ indicates integration over a domain which is fixed in the frame of reference rotating with the vortex system at the turnover period $t_c = 2\pi^2 b^2/\Gamma$. The vorticity center (x_c, y_c) is obtained by :

$$\begin{aligned} x_c &= \frac{\langle \, x\omega_z \, \rangle}{\Gamma} = \frac{\Gamma_x}{\Gamma} \\ y_c &= \frac{\langle \, y\omega_z \, \rangle}{\Gamma} = \frac{\Gamma_y}{\Gamma} \end{aligned} \tag{10}$$

Note that VM2 vortex is more concentrated than a Lamb-Oseen vortex for the same circulation Γ and same size a as shown in Fig. 2.
The Reynolds number based on the circulation $Re_\Gamma = \Gamma/\nu$ and the initial ratio $(a/b)_0$ are shown in Tab. 2 for both 2D and 3D simulations.

3.2 Two-dimensional results / stable merging.

As found by Cerretelli and Williamson[20] and shown by the vorticity contours of Fig. 3, stable merging process can be decomposed into four stages. The two vortices initially turn around each other with the turnover period $t_c = 2\pi^2 b^2/\Gamma$ while the internal vortex core size increases due to the viscous effects. The vortices become rapidly elliptical due to the streching induced by a vortex on its neighbour (see Fig. 3, *a*). During this so-called "first diffusion stage", the vorticity of each vortex is contained in the internal separatrix streamline forming a "8-shaped" loop in the reference frame rotating with the vortex system (Fig. 3, *a*). When this vorticity crosses this separatrix, it is partly advected along the two external streamlines (because of the increase in the vortex core size)(see Fig. 3, *b*). At this point the two vortices start exchanging their vorticity which is the beginning of the second or convective phase. Several vorticity filaments are created at the extremities of the vortex system (Fig. 3, *b*) due to the two re-circulation regions, and the vortices approach each other due to the velocity induced by these filaments on each vortex. The third stage is a second "diffusion phase" where two vorticity extrema persist until they finally merge (Fig. 3, *c*). During the last phase, the vorticity filaments reconnect leading to an increase of vortex core size by viscosity and an axisymmetrisation of the merged vortex (Fig. 3, *d*).
The above description is synthetized in Fig. 4 by the evolution of the separation distance b between the two vortices (whose locations is determined by the local vorticity maximum). It is known that the merging process is highly dependent[14],[19],[20] on the characteristic ratio a/b (a is the dispersion radius Eq. 9). The evolution of a is computed by integration of

the vorticity field in the domain D_i, defined by the orthogonal line of the joing line and the boundaries of the regular domain D_p (see section 3). Fig. 5 shows the evolution of the parameter $(a/b)_0$, for the two initial configurations simulated here and for the different Reynolds numbers considered.

The two co-rotating vortices turn around each other while the characteristic ratio a/b does not reach a threshold value $(a/b)_c$. This critical ratio is determined when the separation distance starts to decrease and corresponds to the beginning of the exchange of vorticity between the two vortices. According to the numerical simulations, this threshold value is $(a/b)_c \sim 0.24$ (Fig. 5, *b*) either for the VM2 and Lamb-Oseen initial vortex system (Fig. 5, *a*) and for all two-dimensional configurations. Furthermore, this value is in agreement with the result of Meunier[19,24] *et al.* and Leweke[14] *et al.*.

A correlation has been derived between the first diffusion time $t_1^* = t_1/t_c$ (*i.e* the time needed by the vortex system to reach the threshold ratio) and the Reynolds number, the initial and threshold ratio, $(a/b)_0$ and $(a/b)_c$:

$$t_1^* = \frac{Re_\Gamma}{8\pi^2 b_0^2} K_d \left(a_c^2 - a_0^2\right) \tag{11}$$

where K_d is a constant extracted from the numerical results (Fig. 5). Its value is $K_d = 0.83 \pm 0.03$ for all the simulations initialized with a vortex system characterized by the initial ratio $(a/b)_0 = 0.1$. The "theoretical value" of this constant is $K_d = 1$ corresponding to the diffusion evolution of an isolated "axisymmetric" gaussian vortex[2] .

The second phase of merging process is approximatively constant $\Delta t_2^* \sim 0.5$ and a part is clearly independent of the Reynolds number as shown in Fig. 4. The evolution of the separation distance b can be approximate as $b(t^*)/b_0 = -3.25t^* + constant$ from a diminution of 20% of separation distance (constant= 0.8). This stage is called "convective phase".

The third phase starts when the separation distance is close to $b/b_0 \sim 0.3$ and corresponds to a diffusion process of vorticity coupled with the rotation of the vortex center. It leads to an axisymmetrization of the vortex center at a time scaling[24] as $Re^{1/2}$. The duration of this "second diffusive" stage has been found from the numerical results to be: $\Delta t_3^* = \alpha Re^{1/2}$ with $\alpha = 8.10^{-3} \pm 1.10^{-3}$.

In order to analyze the structural evolution of one vortex, the tangential velocity profile is determined through the radial circulation profile. This profile is found by interpolating the vorticity field on a polar grid. The vorticity field is integrated on this polar grid, which provides the circulation profile as a function of the radius taken from the vortex center :

$$\Gamma(r) = \int \omega(r,\theta) r dr d\theta \tag{12}$$

Then, the tangential velocity profile is determined by:

$$v_\theta(r) = \frac{\Gamma(r)}{2\pi r} \tag{13}$$

For the simulations initialized by a VM2 vortex system $(a/b)_0 = 0.1$ and $Re_\Gamma = 1500$, the velocity profile evolves towards a profile described by one length scale, as shown in Fig. 6 (note that this process is faster than merging which is attained at $t^* = 1.7$). The intermediate region of the VM2 vortex model (see Fig. 7) vanishes due to the diffusion process of the internal vortex region coupled with the strain field exerted by the second vortex. The internal radius a_1 increases while the external radius a_2 remains constant. For this configuration and both vortex systems, the velocity profile is similar at time $t^* = t/t_c \sim 0.66$ just before the "convective phase" of the merging process, as shown in Fig. 6.
For the simulations initialized by a VM2 and Lamb-Oseen vortex system $(a/b)_0 = 0.1$ and for a Reynolds number $Re_\Gamma = 1500$, the tangential velocity profile of the merged vortex is normalized by the initial $v_{\theta max}$ and plotted in Fig. 7 as a function of the radius normalized by the initial vortex separation distance b_0. The log-log plot shows that the profile is described by two characteristic length scales. It is similar to a VM2 vortex (see section 3 and Fabre and Jacquin[22] for details), the tangential velocity follows a power law $r^{-0.6}$ in the intermediate zone of profile. This profile is extracted when the final vortex is characterized by only one core (one vorticity extremum).
The same result is observed for all two-dimensional simulations and both two initial condition cases (either Lamb-Oseen and VM2 vortices), the Reynolds number has no effect on the structure of the merged vortex. According to these results, the velocity profile of the vortex merged seems to be intrinsic to the stable merging process.

3.3 Three-dimensional results / unstable merging

In the extended near-field of an aircraft wake, the merging of the wing tip and flap vortices may be caused by the development of 3D short wavelength instabilities,[14],[15],[16] . Indeed, in some cases depending on the Reynolds number and on the relative position of the two co-rotating vortices, each vortex becomes unstable with respect to three-dimensional disturbances,[14],[21] . In the real aircraft wake, this instability is characterized by short wavelengths of the order of the vortex core radius a. The wake is modelled to a good approximation as a pair of parallel co-rotating vorticity tubes with the same core size a and circulation Γ.
In order to trigger three-dimensional instabilities, a random white noise is added to the transverse velocity components (u, v) with an amplitude A that does not exceed 1×10^{-3} of the maximum velocity of the base flow :

$$u_0 = u \times (1 + rA);\ v_0 = v \times (1 + rA);\ w_0 = 0 \tag{14}$$

where $r \in [-1/2, 1/2]$ is an uniform random number.
The configuration stutied for the unstable merging is characterized by an initial ratio $(a/b)_0 = 0.15$ and two Reynolds number were considered. Direct Numerical Simulations (DNS) was performed for $Re_\Gamma = 10000$ and Large Eddy Simulation (LES) for $Re_\Gamma = 240000$ using the model described in section 2.2.

When increasing the Reynolds number, the growth of the vortex cores is sufficiently slow for the development of 3D short wavelength instabilities while the two vortices are still separated. These instabilities lead to the unstable merging as shown by the sequence (Fig. 8) by means of the isocontours and isosurfaces of the vorticity magnitude.
The linear regime of the instability development is characterized by an exponential growth of the unstable modes, and by an oscillation of the local position of the vortex cores in the axial direction z (Fig. 8, $t^* = t/t_c \sim 1.95$). This oscillation is characterized by a wavelength corresponding to the wavelength of the mode with the highest growth rate (called most unstable mode). Four wavelengths of the instability are observed at time $t^* = t/t_c \sim 1.95$ in the case of Lamb-Oseen initial vortices and only three wavelengths in case of VM2 initial vortices (Fig. 8). When the unstable modes saturate the flow becomes turbulent ($t^* = t/t_c \sim 2.45$), and the two vortices exchange rapidly their vorticity. Then a merged vortex is obtained by a re-organization/re-laminarization of the turbulent structures ($t^* = t/t_c \sim 3.25$). Note that the global dynamic flow is the same for the two types of initial conditions used (Lamb-Oseen and VM2 vortex model).
A spectral analysis has been performed with the purpose to study the evolution of the kinetic energy contained in all Fourier modes of the domain D. A FFT (Fast Fourier Transform) was performed to determine the characteristic wavelength of the instability and to extract its growth rate during the linear regime (Eq. 15). The related growth rate can be determined from the Fourier decomposition of the total kinetic energy :

$$\sigma = \frac{dln(\widehat{Ec_k^{1/2}})}{dt} \tag{15}$$

where $\widehat{Ec_k^{1/2}}$ is the Fourier coefficient of $Ec^{1/2}$ corresponding to the axial mode of wavenumber k. The random white noise enables the natural amplification of the unstable mode in the vortices which may correspond to the elliptic modes.
In the case of Reynolds number $Re_\Gamma = 10000$, the first mode amplified for the simulation initialized by Lamb-Oseen vortices, is the axial mode $k = 3$ corresponding to the wavelength $\lambda/a = L_z/ka = 3.29$. The normalized growth rate (Fig. 9) of this mode $\sigma_3^* = \sigma_3\, t_c = 3.4$ agrees with the theoretical prediction[16] $\sigma_{th}^* = 3.47$, based on the linear stability theory derived for a Gaussian vortex. However, the mode $k = 4$ ($\lambda/a = 2.46$) is amplified afterwards, with a growth rate $\sigma_4^* \sim 5$ (Fig. 8, $t^* = 1.95$). This mode is not predicted by the theory for this configuration. This can be explained by the viscous effects modifying the vortex core in the low Reynolds conditions. Indeed, the vortex core size a increases by a diffusive process and the ratio a/b is higher than the initial ratio used for the theoretical prediction. Therefore the analytical prediction has been made using the instantaneous value of the ratio $a/b = 0.178$ reached at the beginning of the linear phase and the mode $k = 4$ correctly appears to be an unstable mode. However in this case the theoretical growth rate $\sigma_{th}^* = 2.47$ is smaller than the numerical one $\sigma_4^* \sim 5$ (Fig. 9). This can be explained by the fact that both modes $k = 3$ and $k = 4$ are already amplified.

Thus, the energy evolution following the initial amplification of the mode $k = 3$ does not correspond to an ideal situation of a linear regime with the exponential growth of a single mode of the short wavelength instability.
In the case of the simulation initialized with VM2 vortices, the most unstable mode governing the dynamics, is the axial Fourier mode $k = 3$ corresponding to a wavelength $\lambda/a = 3.29$ (Fig. 8, $t^* = 1.95$). As shown by the figure 9, the process observed in the previous case is inversed, the axial mode $k = 4$ is the first most unstable mode amplified then the mode $k = 3$ is amplified with a growth rate $\sigma_3^* = 6.5$. The unstable mode of the short wavelength instability which develops in the configuration with VM2 vortices saturates weakly before the one with Lamb-Oseen vortices.
The three-dimensional simulation at high Reynolds number $Re_\Gamma = 240000$ shows the same flow dynamics as the previous case. In the case of an initial condition generated with Lamb-Oseen vortices, the most unstable mode is the mode $k = 3$ and the corresponding wavelength is $\lambda/a = 3.29$, as predicted by the theory of Le Dizes and Laporte[16] . Furthermore the numerical growth rate $\sigma_3^* \sim 4.5$ (Fig. 9) is in good agreement with the prediction $\sigma_{th}^* = 4.75$. In the case of VM2 initial vortices, the most unstable mode of the elliptic instability is the mode $k = 7$ and the corresponding wavelength is $\lambda/a = 1.41$. Its numerical growth rate is $\sigma_7^* \sim 6$ (Fig. 9) and is higher of 33% than the growth rate of the instability in Lamb-Oseen vortices. The most unstable mode saturates earlier in the case with VM2 initial vortices. This difference between the two cases of the initial condition, can be explained by the fact that the selection of the unstable mode is based on the axial length of the computational domain, which was determined using the theoretical prediction of the short wavelength instability for Gaussian vortices, whereas the VM2 model does not correspond to a Gaussian vortex.
A plane containing the mean values of the velocity (averaging in axial direction) is used to determine the evolution of both the characteristic ratio a/b and the separation distance b/b_0, and also to extract the velocity profile of the merged vortex. The same method as in two-dimensional simulations is used to extract these results. Note that the turbulence generated when the unstable mode saturates, complicates the tracking of the evolution of these two characteristic parameters due to the presence of small scale structures generated by the loss of coherence of the two vortices and which have turbulent motions. The use of these parameters are not entirely appropriate here. Nervertheless a comparison with the two-dimensional simulation (stable merging) of the characteristic parameter b/b_0 is made (Fig. 10).
The main result is that the unstable merging is quicker than the stable merging. Indeed the stable merging is reached at the normalized time $t^* \sim 5.1$ and the unstable merging at $t^* \sim 3.2$. The development of short wavelength instability is responsible for the early merging of the two co-rotating vortices.
The tangential velocity profiles of the merged vortex are plotted in Fig. 11 for the simulation at $Re_\Gamma = 10000$ and in Fig. 11 at $Re_\Gamma = 240000$. This profile is described by two length scales as a VM2 vortex. However the tangential velocity follows a power law

of $v_\theta \sim r^{-\alpha}$ with $\alpha = 0.35$ in the intermediate region defined by the two length scales. The velocity profile of the final vortex has the same structure for the two Reynolds number considered and equally for the two initial configurations considered (Fig. 11). The Reynolds number seems to have no effect on the structure of the vortex core, which was also observed in the case of two-dimensional/stable merging. Both for the two initial vortex models (Lamb-Oseen and VM2), the profile of the final vortex is almost identical, as the results obtained in the case of stable merging (sec. 3.2). The structure of the final vortex core seems to be an intrinsic result of the merging process.

4 CONCLUSION

The main interest of this study was to investigate extensively by means of DNS and LES, the effect of Reynolds number on the merging phenomenon and on the structure of the final vortex. The results reinforces the conclusion that the merging process of two co-rotating vortices is controlled by the characteristic ratio a/b between the vortex core size a and the separation distance b.

The stable merging (2D) was studied for different Reynolds numbers ($750 < Re_\Gamma < 10000$) by Direct Numerical Simulation (DNS). These simulations performed showed that the merging process takes place when the two vortices begin to exchange their vorticity. This exchange starts when the characteristic ratio a/b reaches the critical value $a/b)_c \sim 0.24$. The results showed the same global dynamics of the stable merging for the Reynolds numbers considered here and for both initial condition (Lamb-Oseen and Jacquin VM2 vortex models). The Reynolds number has no effect on the structure of the final vortex core, characterized by a tangential velocity profile similar to a Jacquin VM2 vortex (described by two characteristics length scales). The effect of increasing the Reynolds number is to increase the number of vortex system revolution has to encounter before the merging.

On the other hand, the unstable merging (3D) was simulated using a temporal DNS for the Reynolds number $Re_\Gamma = 10000$ and temporal Large-Eddy Simulation (LES) for $Re_\Gamma = 240000$. The three-dimensional simulation showed that a cooperative short wavelength instability can develop in the vortex core due to the strain field which is induced by one vortex on its neighbour. This instability is responsible of the unstable merging of the two co-rotating vortices.The numerical results at high Reynolds number are in agreement with the theoretical prediction of Le Dizes and Laporte[16] for the development of short wavelength instability. It was also observed that the growth rate of the instability development for the VM2 vortices is higher than the one of Lamb-Oseen vortices. The final vortex resulting to the unstable merging has the same tangential velocity profile for both initial conditions considered.

In both stable and unstable merging, the structure of the final vortex core seems to be intrinsic to the merging process and characterized by a velocity profile with two characteristic length scales as a VM2 vortex. If the Reynolds number increases, the stable merging will occur later and then giving the opportunity to develop a short wavelength instability conducing to the unstable merging.

Domaine D	L_x	x_{min}	x_{max}	n_{tot}	Zone D_p	L_{xp}	x_{start}	x_{end}	n_p
	$20b_0$	$-10b_0$	$10b_0$	401		$2.4b_0$	$-1.2b_0$	$1.2b_0$	342

Table 1: Charateristics of the computational domain and the mesh grid.

Re_Γ	750	1500	5000	10000	240000
$(a/b)_0 = 0.1$	$DNS-2D$	$DNS-2D$	$DNS-2D$		$DNS-2D$
$(a/b)_0 = 0.15$				$DNS-2D/3D$	$LES-3D$

Table 2: Numerical configurations

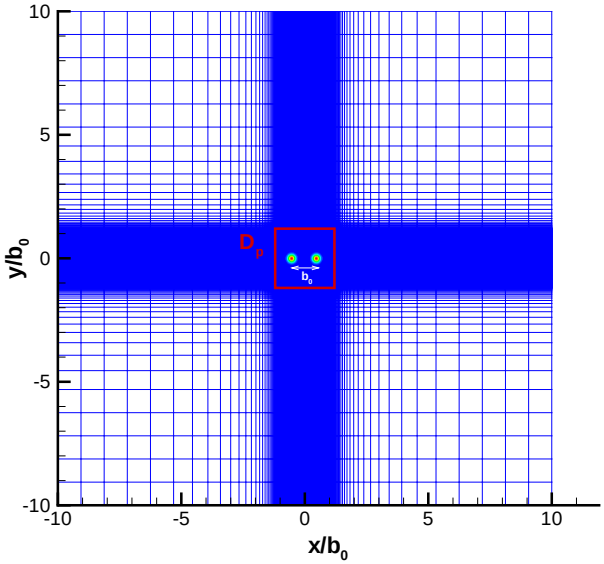

Figure 1: Domain, mesh and vortex initial position (colors points). The axis are normalized by the initial separation distance b_0 of the two co-rotating vortices.

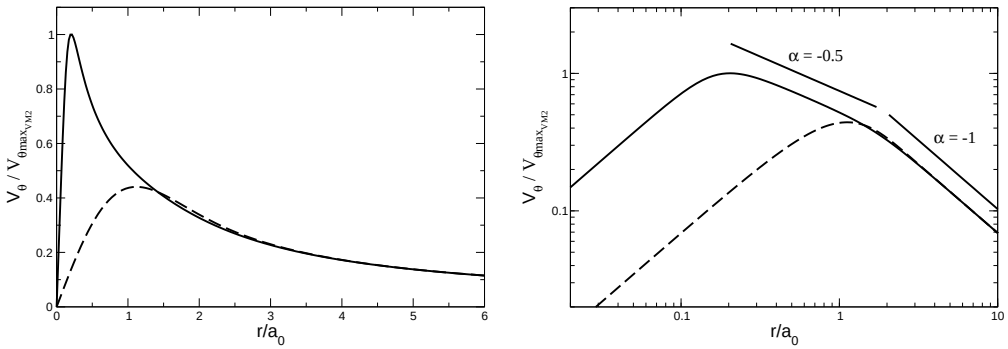

Figure 2: Tangential velocity profile of a VM2 Jacquin (solid line) and Lamb-Osen (dashed line) vortex. The velocity is normalized by the initial maximun tangential velocity of the VM2 vortex, and the distance r by the initial dispersion radius a_0.

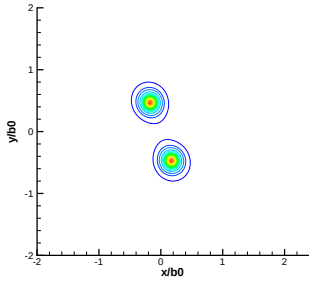

a) First diffusion stage $t^* = t/t_c = 0.19$

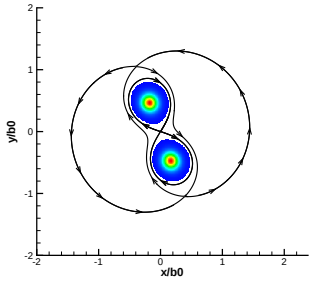

Separatrix streamlines (bold lines) and vorticity

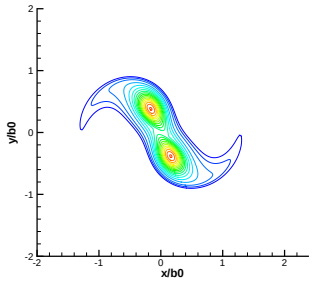

b) Convective stage $t^* = t/t_c = 1.1$

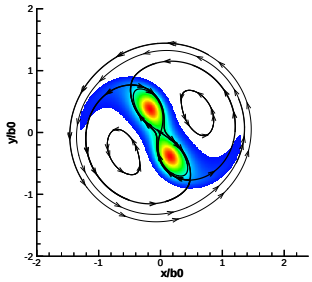

Separatrix streamlines (bold lines) and vorticity

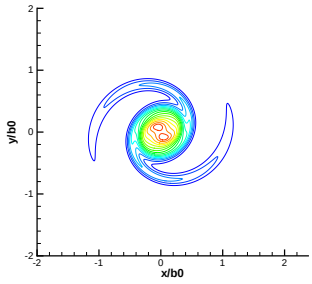

c) Second diffusion stage $t^* = 1.52$

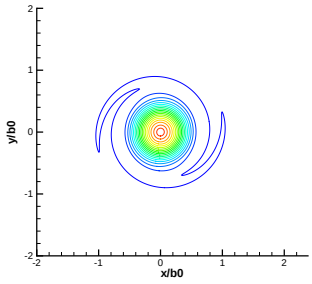

d) "Axisymmetrization" phase $t^* = 2.02$

Figure 3: Isocontours of vorticity magnitude $||\vec{\omega}||$: the dynamic flow of the stable merging with VM2 vortex model as initial condition. Vorticity is clockwise.

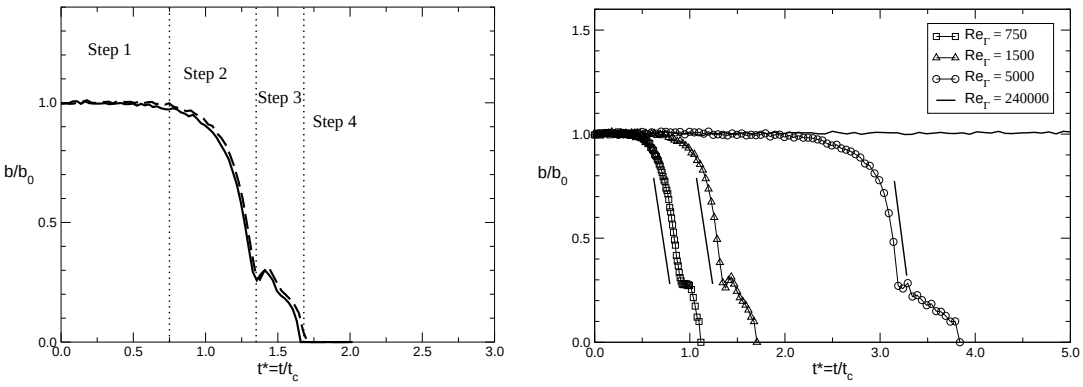

Figure 4: Evolution of the nondimensional separation distance b/b_0. Left: Configuration $(a/b)_0 = 0.1$, $Re_\Gamma = 1500$ and both VM2 (solid line) and Lamb-Oseen (dashed line) vortex model as initial numerical condition. Right: same, as a function of the Reynolds number.

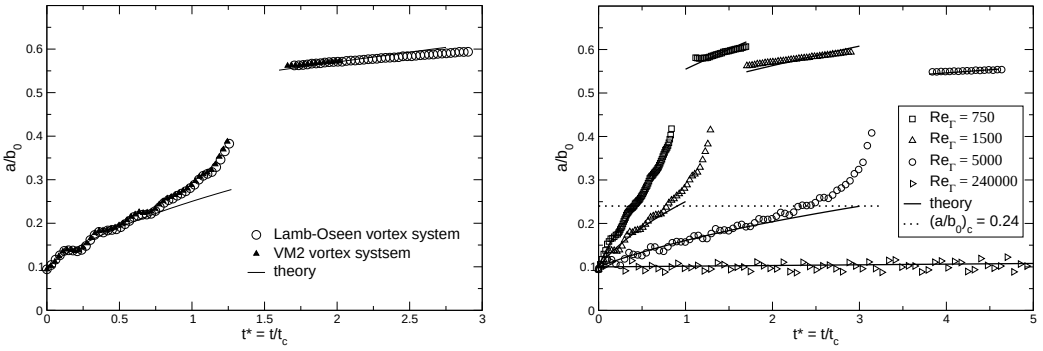

a)Comparison of the two initialisations cases and $Re_\Gamma = 1500$.

b)Reynolds number effects with an initial Lamb-Oseen vortex system.

Figure 5: Evolution of the characteristic ratio a/b. Initial configuration $(a/b)_0 = 0.1$

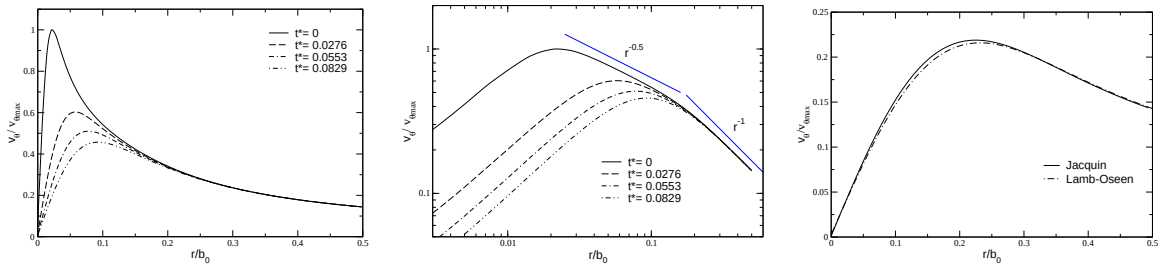

Figure 6: Tangential velocity profile (initial configuration $(a/b)_0 = 0.1$ with VM2 vortex system at $Re_\Gamma = 1500$. Left to right:: the linear velocity profile as a function of the normalized time $t^* = t/t_c$ $Re_\Gamma = 1500$, the corresponding log-log plots, and a comparison of the velocity profile at $t^* \sim 0.66$ for the two initial vortex system. ($v_\theta(r)$ is normalized by the initial tangential velocity maximum $v_{\theta max}$ and the distance from the center r by the initial separation distance b_0.)

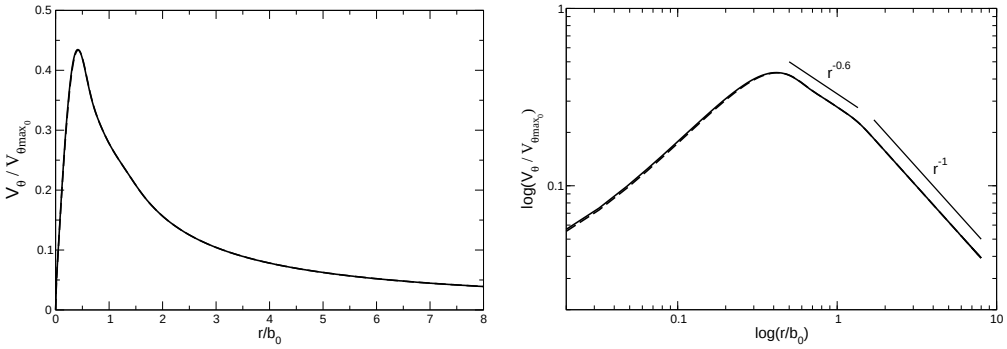

Figure 7: Tangential velocity profile of the final vortex at $t* = t/t_c \sim 1.7$: linear (at right) and log-log plots (at right). Initial configuration $(a/b)_0 = 0.1$ and $Re_\Gamma = 1500$. The initial tangential velocity maximum $v_{\theta max}$ is used to normalize the velocity and the distance from the center r by the initial separation distance b_0.

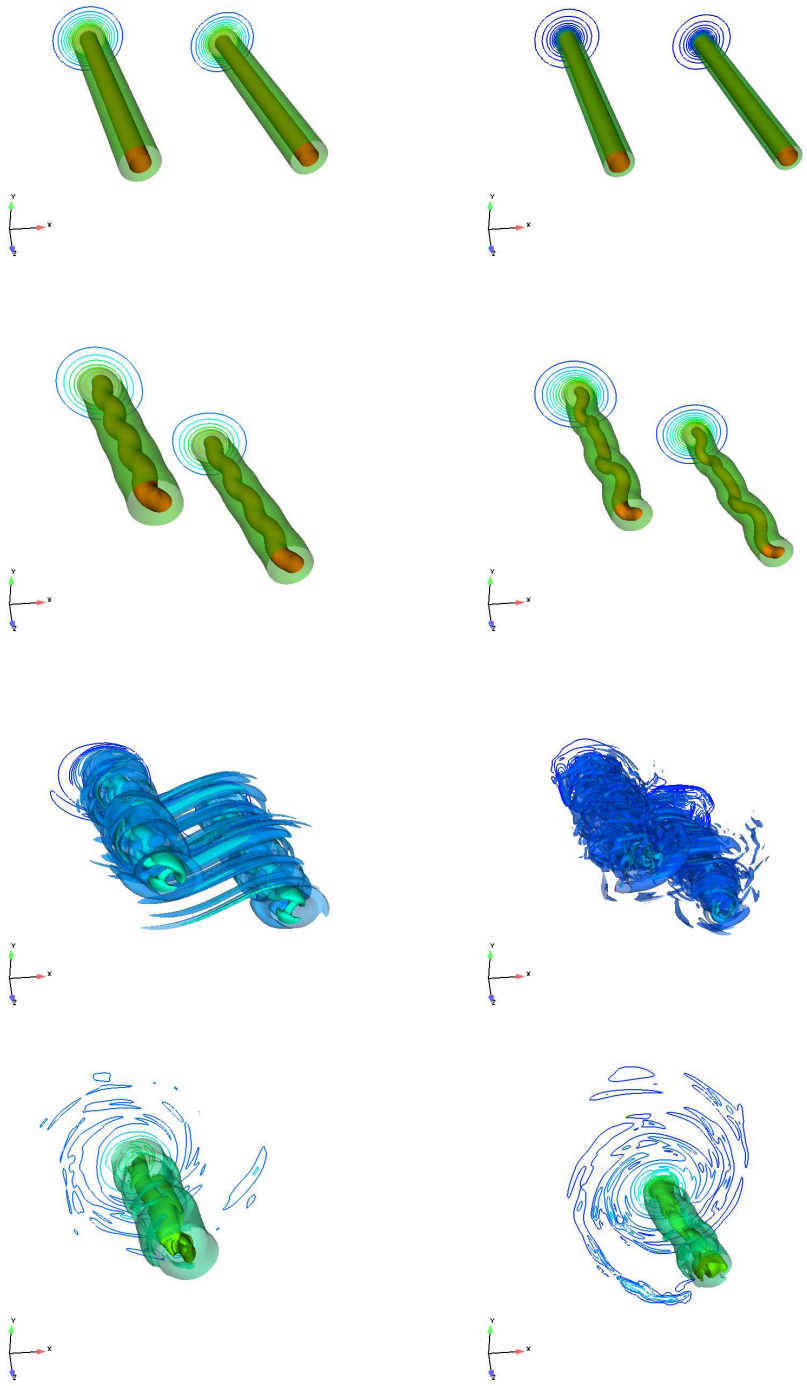

Figure 8: Dynamic flow of the unstable merging illustrates by isocontours of vorticity magnitude $||\vec{\omega}||$. Left part: initial Lamb-Oseen vortex system and on right part: initial VM2 vortex system. Vorticity is clockwise. Configuration $(a/b)_0 = 0.15$ and $Re_\Gamma = 10000$. Top to bottom : $t^* = t/t_c \sim 0, 1.95, 2.45, 3.25$.

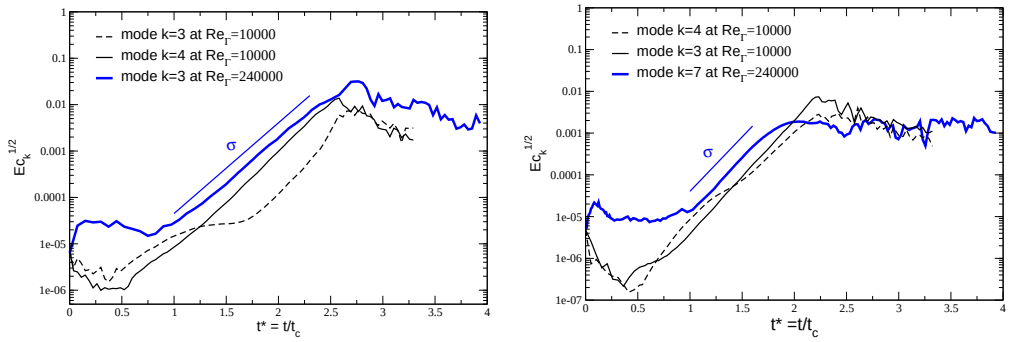

Figure 9: Spectral energy of the unstable mode k function to the normalized time $t^* = t/t_c$. Left: initial Lamb-Oseen vortex system, and right: VM2 initial vortex system.

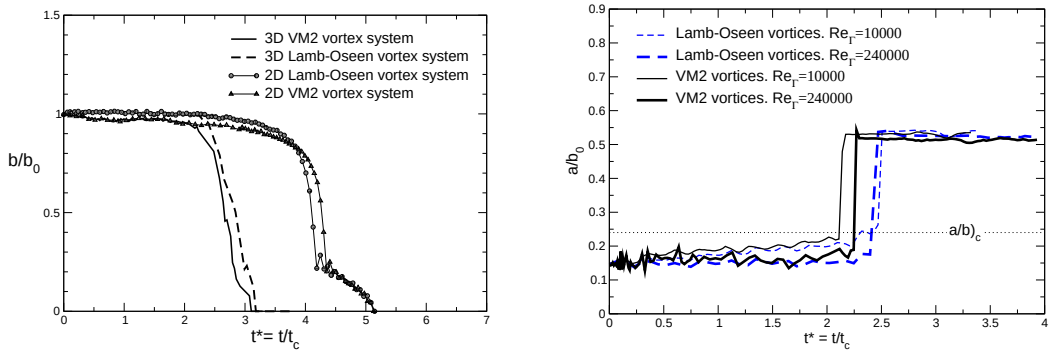

Figure 10: Evolution of the characteristic parameters: right, the separation distance b ($Re_\Gamma = 10000$) and left, the ratio a/b for the two 3D simulations, as a function to the normalized time $t^* = t/t_c$.

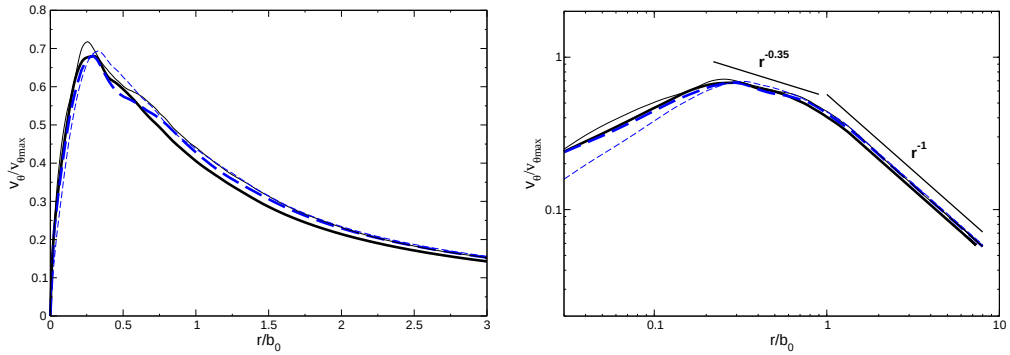

Figure 11: Velocity profile of the merged vortex resulting to the three-dimensional simulations. Dashed line for an initial Lamb-Oseen vortex system and solid line for a VM2 vortex system. Thick line at $t^* = t/t_c \sim 3.25$ and $Re_\Gamma = 10000$ and thin line at $t^* = t/t_c \sim 3.93$ for $Re_\Gamma = 240000$.

REFERENCES

[1] H. Lamb. Hydrodynamics. *6^{th} ed. Cambridge Univ. Press*, (1932).

[2] P.G. Saffman. Vortex Dynamics. *Cambridge University Press*, (1992).

[3] S.K. Lele. Compact finite difference scheme with spectral-like resolution. *J. Comput. Phys.*, **103**, 16–42, (1992).

[4] T.J. Poinsot and S.K. Lele. Boundary Conditions for Direct Simulations of Compressible Viscous Flows. *J. Comput. Phys.*, **101**, 104–129, (1992).

[5] G. Erlebacher, M.Y. Hussaini, C.G. Speziale and T. A. Zang. Towards the Large-Eddy Simulation of Compressible Turbulence. *J. Fluid Mech*, **238**, 155–185, (1992).

[6] O. Métais and M. Lesieur. Spectral Large-Eddy Simulation of Isotropic and Stably Stratified Turbulence. *J. Fluid Mech.*, **239**, 157–194, (1992).

[7] . S. Ragab and M. Sreedhar. Numerical simulation of vortices with axial velocity profiles. *Phys. Fluids*, **7**, 549–558, (1994).

[8] F. Ducros, P. Comte and M. Lesieur. Large-eddy simulation of transition to turbulence in a boundary layer spatially developing over a flat plate. *J. Fluid Mech.*, **326**, 1–36, (1996).

[9] P. Spalart. Airplane Trailing Vortices. *Ann. Rev. Fluid Mech.*, (1998).

[10] T. Leweke and C.H.KWilliamson. Cooperative elliptic instability of a vortex pair. *J. Fluid Mech.*, **360**, 85–119, (1998).

[11] L. Gamet, F. Ducros, F. Nicoud and T. Poinsot. Compact finite difference schemes on non-uniform meshes. Application to direct numerical simulations of compressible flows. *Int. J. Numer. Meth. Fluids*, **29**, 159–191, (1999).

[12] F. Laporte and A. Corjon. Direct Numerical Simulations of the elliptic instability of a vortex pair. *Phys. Fluids*, **12**, 1016–1031, (1999).

[13] L. Jacquin, D. Fabre, P. Geoffroy and E. Coustols. The Properties of a Transport Aircraft Wake in the Extended Near Field: an Experimental Study. *AIAA Paper 2001-1038*, **1038**, (2001).

[14] T. Leweke, P. Meunier, F. Laporte and D. Darracq. Controlled interaction of co-rotating vortices. *ONERA-DLR Aerospace Symposium ODAS*, (2001).

[15] P. Meunier and T. Leweke. Three-dimensional instability during vortex merging, *Phys. Fluids*, **13**, 2747–2750, (2001)

[16] S. Le Dizes and F. Laporte. Theorical prediction for elliptical instability in a two-vortex flow. *J. Fluid Mech.*, **47**, 169–201, (2002).

[17] F. Laporte. Application of the numerical simulation to the characterization and the instabilities of transport aircraft wake vortices. *PhD thesis, Institut National Polytechnique de Toulouse, CERFACS, France*, (2002).

[18] S. Le Dizes and A. Verga. Viscous interactions of two co-rotating vortices before merging. *J. Fluid Mech.*, **467**, 389–410, (2002).

[19] P. Meunier, Ehrenstein, T. Leweke and M. Rossi. A merging criterion for two-dimensional co-rotating vortices. *Phys. Fluids*, **14**, 2757–2766, (2002).

[20] C. Cerretelli and C.H.K. Williamson. The physical mechanism for vortex merging, *J. Fluid Mech.*, **475**., 41–77, (2003).

[21] H. Moet. Numerical simulation of the behaviour of aircraft wake vortices in the atmosphere. *PhD thesis, Institut National Polytechnique de Toulouse, CERFACS, France*, (2003).

[22] D. Fabre D. and L. Jacquin. Short-wave cooperative instabilities in representative aircraft vortices. *Phys. Fluids*, **16**, No. 5, 1366–1378, (2004).

[23] Paulo J.S.A. Ferreira de Sousa, J.C.F. Pereira. Reynolds number dependence of two-dimensionnal laminar co-rotating vortex merging. *Theo. and Comp. Fluid Dynamics*, **19**, 65–75, (2005).

[24] P. Meunier, S. Le Dizes and T. Leweke. Physics of merging. *C.R. Physique*, **6**, (2005).